

Electron spin resonance matrix isolation studies of ^{27}Al , ^{17}O , $^{69,71}\text{Ga}$, $^{16,17}\text{O}$ and ^{115}In , $^{16,17}\text{O}$: Observed hyperfine interactions compared with ab initio theoretical results

Lon B. Knight Jr., Thomas J. Kirk, John Herlong, John G. Kaup, and E. R. Davidson

Citation: *The Journal of Chemical Physics* **107**, 7011 (1997); doi: 10.1063/1.475164

View online: <http://dx.doi.org/10.1063/1.475164>

View Table of Contents: <http://scitation.aip.org/content/aip/journal/jcp/107/18?ver=pdfcov>

Published by the [AIP Publishing](#)

Articles you may be interested in

[Electron spin resonance g tensors for complexes of Ne and Ar with AlO: Theoretical studies related to the large matrix effect observed for AlO](#)

J. Chem. Phys. **122**, 124504 (2005); 10.1063/1.1866095

[Matrix-isolation investigation of the diatomic anion radicals of aluminum and gallium \(\$\text{Al}^{2-}\$ and \$\text{Ga}^{2-}\$ \): An electron spin resonance and ab initio theoretical study](#)

J. Chem. Phys. **115**, 4632 (2001); 10.1063/1.1389841

[Ab initio and molecular-dynamics studies on rare gas hydrides: Potential-energy curves, isotropic hyperfine properties, and matrix cage trapping of atomic hydrogen](#)

J. Chem. Phys. **110**, 11814 (1999); 10.1063/1.479173

[Electron spin resonance studies of \$^{45}\text{Sc}\$, \$^{17}\text{O}\$, \$^{89}\text{Y}\$, \$^{17}\text{O}\$, and \$^{139}\text{La}\$, \$^{17}\text{O}\$ in rare gas matrices: Comparison with ab initio electronic structure and nuclear hyperfine calculations](#)

J. Chem. Phys. **110**, 5658 (1999); 10.1063/1.478464

[Neon and argon matrix ESR and theoretical studies of the \$^{12}\text{CH}_3\text{Cd}\$, \$^{12}\text{CD}_3\text{Cd}\$, \$^{13}\text{CH}_3\text{Cd}\$, \$^{12}\text{CH}_3^{111}\text{Cd}\$, and \$^{12}\text{CH}_3^{113}\text{Cd}\$ radicals](#)

J. Chem. Phys. **110**, 3398 (1999); 10.1063/1.478206



Electron spin resonance matrix isolation studies of $^{27}\text{Al}^{16,17}\text{O}$, $^{69,71}\text{Ga}^{16,17}\text{O}$ and $^{115}\text{In}^{16,17}\text{O}$: Observed hyperfine interactions compared with *ab initio* theoretical results

Lon B. Knight, Jr., Thomas J. Kirk, John Herlong, and John G. Kaup
Chemistry Department, Furman University, Greenville, South Carolina 29613

E. R. Davidson
Chemistry Department, Indiana University, Bloomington, Indiana 47405

(Received 10 June 1997; accepted 6 August 1997)

Electron spin resonance (ESR) studies are reported for $\text{Al}^{16,17}\text{O}$, $\text{Ga}^{16,17}\text{O}$, and $\text{In}^{16,17}\text{O}$ isolated in neon matrices at 4 K. Except for Al^{16}O , no previous ESR measurements have been reported for these $X\ ^2\Sigma$ diatomic radicals. The pulsed laser vaporization of the metals in the presence of $^{16}\text{O}_2$ and $^{17}\text{O}_2$ produced high quality ESR spectra of these metal oxide radicals whose nuclear hyperfine interactions (A tensors) were fully resolved for both the metal and oxygen nuclei. An analysis of the experimental spin densities in combination with different types of theoretical calculations provided detailed information concerning the electronic structure trends going down this metal oxide group. Increased *p*-orbital spin density on oxygen was observed for the heavier metal oxide radicals. Nonrelativistic *ab initio* calculations with an extended basis set and the UB3LYP method reproduced the trends in the isotropic and dipolar hyperfine interactions. All-electron CI calculations, restricted open-shell Hartree–Fock (ROHF) wave functions, and unrestricted Hartree–Fock wave functions gave results very different from experiment and from each other for the isotropic interaction. All calculations were in fair agreement with each other for the dipolar interaction and provided an assignment of the sign for that term. © 1997 American Institute of Physics. [S0021-9606(97)01942-9]

I. INTRODUCTION

Understanding the electronic structures of “simple” metal oxides is important for several reasons, especially given their involvement in superconducting materials and thin film insulators. For this vertical series of increasingly complex and isovalent $X\ ^2\Sigma$ metal oxide diatomic radicals, the nuclear hyperfine interactions reveal interesting trends for the valence electronic structure region. It is especially significant to develop computational methods which can be tested directly on such prototypical species, thus increasing the reliability of theoretical predictions for the more complex materials for which direct hyperfine and other measurements cannot readily be made. Metal oxide (MO) formation is often a critical factor in chemical vapor deposition (CVD) processes which are used to produce a wide variety of coatings for microelectronic devices.

This study reports and analyzes the first electron spin resonance (ESR) measurements of any kind for gallium oxide (GaO) and indium oxide (InO). Also, the first ^{17}O ($I = 5/2$) hyperfine structure (hfs) measurements for aluminum oxide (Al^{17}O) are reported, although the ^{27}Al hfs for $^{27}\text{Al}^{16}\text{O}$ has been fully resolved in previous matrix studies and in high resolution gas phase experiments.^{1,2} Matrix and gas phase studies have also been reported for the lightest member of this series, namely the boron oxide (BO) molecule.^{3,4} A complete resolution of the hyperfine interactions (A tensors) for the metal atoms and ^{17}O in this MO series was possible. As might be expected, the free atom comparison method (FACM) seemed to be a reasonable approach for the

lighter MO radicals but it was more problematic for the heavier GaO and InO molecules. However, the isotopic (A_{iso}) and dipolar (A_{dip}) components of the hyperfine interactions reveal interesting qualitative trends going down this MO series. In fact, this set of MO radical measurements (BO, AlO, GaO, and InO) represents the most complete vertical profile of spin density results reported to date.

Comparisons are made between the experimental A_{iso} and A_{dip} values and those calculated from unrestricted Hartree–Fock (UHF) and density functional theory (DFT) methods. The unusually large divergence in the A values predicted by these two theoretical methods is discussed in terms of special electronic structure features of these metal oxide radicals. It is most difficult to properly balance contributions to the overall electronic structure from the two ionic extremes of M^+O^- (unpaired electron formally resides on oxygen) and $\text{M}^{++}\text{O}^{--}$ (where it resides on the metal atom). Previous dipole moment calculations have encountered a similar problem for the AlO radical.⁵ This treatment found a gradual transition from Al^+O^- to $\text{Al}^{++}\text{O}^{--}$ in the internuclear distance range of 3 to 4 a.u. The observed nuclear hyperfine properties of these MO radicals is extremely sensitive to the balance of these two different ionic descriptions, thus making ESR measurements especially appropriate. The results of this study should provide a better understanding of ionic metal oxide bonding, especially since only a few cases of this type have been studied previously and none have had their ^{17}O hyperfine properties investigated. Also in several cases where metal oxides have been observed, for example ScO and YO,⁶ the metal hyperfine interactions were not re-

solved into parallel and perpendicular components, thus preventing a direct determination of the separate “*ns*” and “*np*” or “*nd*” orbital contributions.

A considerable number of gas phase electronic transitions have been analyzed for this group IIIA diatomic metal oxide series.⁷ In more recent experiments, the Al_2O molecule has been prepared by the oxidation of laser vaporized aluminum and studied under supersonic beam conditions.⁸ Thermochemical studies of AlO and AlO^+ with various reactants have also been made in the gas phase,^{9–12} as well as reactive quenching of electronically excited AlO .¹³ Properties of AlO are especially interesting given its presence in a wide range of high temperature environments from rocket exhausts and explosives to upper atmospheric monitoring and astrophysical and geophysical applications. (See Refs. 8–10 and 14–17.) In earlier experiments, laser ablated Al atoms and AlO from Al_2O_3 surfaces were used to study the laser ablation mechanism.¹⁸

It is interesting that recent vibrational studies of reactions between laser ablated gallium and indium metals with O_2 in argon matrices did not detect the direct presence of the monoxide radicals, however GaO_2 and InO_2 were clearly observed.¹⁹ The vibrational matrix studies were not conducted in neon matrices. These ESR matrix experiments are consistent with the earlier vibrational studies in that we observed intense GaO and InO absorptions in neon but extremely weak signals for InO and none for GaO in argon matrices. Aluminum and boron reactions under such argon conditions did produce AlO , AlO_2 , BO , and BO_2 . Vibrational matrix studies of a wide variety of M_xO_y species have recently been summarized by Andrews and co-workers, including the earlier matrix work which employed thermal sources of the metal atom in codeposition reactions with O_2 .^{19,20,21–24}

A wide variety of neutral and charged radicals can be studied in rare gas matrices by ESR. Weltner’s review of the ESR matrix method includes a listing of the diatomic metal oxides studied in earlier years— RbO , CsO , BO , AlO , ScO , YO , LaO , VO , NbO , MnO , and GdO .²⁵ Dioxides studied by this method include MnO_2 ,²⁵ PO_2 , AsO_2 ,²⁶ and VO_2 .²⁷ Recently studied small radicals relevant to this AlO , GaO , and InO series include AlH^+ ,²⁸ AlF^+ ,²⁹ AlC ,³⁰ AlH_2 ,³¹ Al_3 ,³² HAICH_3 ,³³ $\text{Al}(\text{CO})_2$,³⁴ GaAs^+ ,³⁵ Ga_3 ,³⁶ GaH_2 ,³⁷ Ga_2As_3 ,³⁸ and $\text{Ga}(\text{C}_2\text{H}_4)$.³⁹ Only a small number of gallium centered radicals have been investigated³⁷ and apparently no indium radical ESR studies have been reported, although GaH_2 and InH_2 have been investigated by vibrational spectroscopy in rare gas hosts.⁴⁰

II. EXPERIMENT

The rare gas matrix apparatus used in our laboratory (Furman University) for X-band ESR studies of small radicals has been described previously.^{26–28,41} Both liquid helium and closed cycle helium refrigerators are used in various experimental arrangements to cool the copper matrix deposition surface to 4 to 5 K. Matrix depositions under reactive laser vaporization conditions were conducted by two differ-

ent experimental procedures. One procedure involved the direct passage of pure $\text{O}_2(\text{g})$ over the metal surface (Al, Ga, or In) which was undergoing pulsed laser vaporization. (See Fig. 1 of Ref. 28.) The second harmonic (532 nm) of the Nd:YAG pump laser was focused to a spot size of approximately 0.3 mm. The focused beam was slowly rastered over the surface by means of an external focusing lens. The vaporization laser was operated at 10 Hz and pulse energies of approximately 15 mJ for aluminum, 10 mJ for gallium, and 4 mJ for indium. The high purity metal targets were obtained from Alfa. In this arrangement, the laser ablated reaction products encountered the condensing rare gas in the vicinity of the copper matrix surface which was located 6 cm from the laser vaporization target. A typical rare gas flow rate of 5 sccm (std. $\text{cm}^3 \text{min}^{-1}$) was employed. This flow rate for neon caused the hot-filament type ionization gauge (calibrated for N_2) in the matrix deposition vicinity to indicate a pressure of approximately 5×10^{-5} Torr.

In the direct reaction mode described above (O_2 passed directly over the metal undergoing laser ablation), the amount of O_2 introduced was varied from approximately 1% to 0.01% of the rare gas amount in a series of different depositions, each lasting for 30 min. This same concentration range was also employed in a series of indirect reaction deposition experiments. In the indirect scheme, the O_2 was premixed with the rare gas—hence, no O_2 gas was passed directly over the metal vaporization surface. While there is not complete separation, most metal atom– O_2 encounters occurred during the matrix condensation process in this indirect experimental reaction arrangement.

For both reaction methods, background pressures were typically 5×10^{-7} Torr with water being the predominant contaminant. Background gases and isotopically enriched $^{17}\text{O}_2$ samples, obtained from Isotec, were monitored with a quadrupole mass spectrometer (Stanford Research System RGA200) which is built into the vacuum system of the matrix isolation cryostat.

III. RESULTS: ESR ANALYSIS

The analysis of the observed ESR spectra for AlO , GaO , and InO was straightforward. However, the large magnitude of the metal hyperfine interactions required an exact diagonalization of the determinants resulting from the following spin Hamiltonian:

$$\hat{H} = \beta \vec{H} \cdot \hat{g} \cdot \vec{S} + \vec{S} \cdot \hat{A} \cdot \vec{I},$$

where all symbols have their standard meanings.²⁵ Quadrupole interaction was negligible since this effect decreases as A , the hyperfine tensor, increases. For the allowed $\Delta M_S = +1$ and $\Delta M_I = 0$ transitions, the nuclear Zeeman interaction can also be neglected. The magnetic energy levels resulting from this exact diagonalization treatment at all angles are coupled with a transition probability routine and a Lorentzian lineshape program for simulating the first derivative ESR spectra. These combined programs, written in our

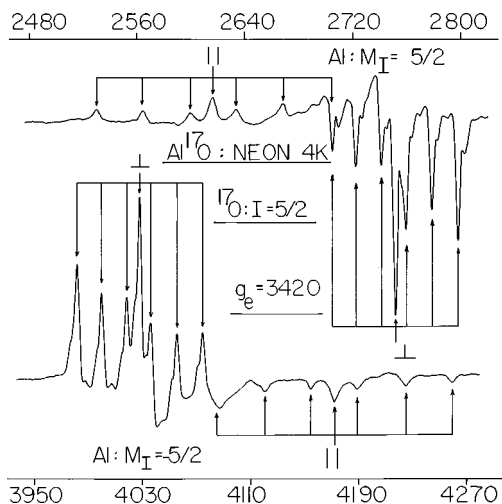


FIG. 1. Sextet $^{17}\text{O}(I=5/2)$ hyperfine structure is shown in the neon matrix ESR spectra of the lowest ($M_I=5/2$) and highest ($M_I=-5/2$) field parallel ($\Theta=0^\circ$) and perpendicular ($\Theta=90^\circ$) transitions of $\text{Al}(I=5/2)$ for the $^{27}\text{Al}^{17}\text{O}$ radical in its $X^2\Sigma$ ground electronic state. The central region of each ^{17}O sextet pattern exhibits a single line resulting from $^{27}\text{Al}^{16}\text{O}$ which has no oxygen splitting. Line positions for AlO are listed in Table I.

laboratory and described previously,⁴¹ were used to obtain all the calculated line positions and simulated ESR spectra presented in this article.

All spectra exhibited random orientation in the rare gas lattice and axial symmetry. Only two molecular g components are involved and for each magnetic nucleus there are only two A tensor components, referred to as A_{\parallel} and A_{\perp} . These molecular magnetic parameters were obtained by fitting the observed and calculated line positions. As discussed below, the ESR spectra for ^{115}InO was especially challenging since “extra” or “off-angle” absorptions were observed whose intensities for some transitions were comparable to the $\Theta=0^\circ$ and $\Theta=90^\circ$ limits of the various hyperfine transitions. Theta “ Θ ” is defined as the angle between the molecular axis of these diatomic radicals and the externally applied magnetic field.

A. $^{27}\text{Al}^{16,17}\text{O}$

The neon matrix ESR spectra for $^{27}\text{Al}^{16}\text{O}$ consisted of aluminum ($I=5/2$) sextets of parallel ($\Theta=0^\circ$) and perpendicular ($\Theta=90^\circ$) absorptions with linewidths of approximately 1 to 2 Gauss. The lowest ($M_I=5/2$) and highest ($M_I=-5/2$) field absorptions for a mixture of $^{27}\text{Al}^{16}\text{O}$ and $^{27}\text{Al}^{17}\text{O}$ are shown in Fig. 1. Note the consistent phase relationships and the $^{17}\text{O}(I=5/2)$ sextet hyperfine structure for both the perpendicular and parallel components. The observed ESR line positions for AlO in neon at 4 K are listed in Table I and the extracted magnetic parameters are presented in Table III.

B. $^{69,71}\text{Ga}^{16}\text{O}$ and $^{69,71}\text{Ga}^{17}\text{O}$

Gallium has two magnetic isotopes, ^{69}Ga (60% nat'l abund., $I=3/2$, $\mu_I=2.0145$ nm) and ^{71}Ga (40%, $I=3/2$, $\mu_I=2.5597$ nm). The neon matrix ESR spectrum assigned to

TABLE I. ^aObserved ESR line positions (Gauss) for $^{27}\text{Al}^{16}\text{O}$ in neon matrix at 4 K.

$^{27}\text{Al}:I=5/2$	Perpendicular ($\theta=90^\circ$)	Parallel ($\theta=0^\circ$)
$M_I=5/2$	2750	2614
3/2	2956	2886
1/2	3188	3178
-1/2	3443	3490
-3/2	3722	3820
-5/2	4026	4171

^aMicrowave frequency is 9570.9(4) MHz. Calculated line positions agree with these observed lines within the experimental uncertainty of ± 1 G. Additional $^{17}\text{O}(I=5/2)$ hfs for AlO was also observed. See magnetic parameters listed in Table III and spectra in Fig. 1.

$^{69}\text{Ga}^{16}\text{O}$ and $^{71}\text{Ga}^{16}\text{O}$ in Fig. 2 reflects these isotopic characteristics, with each isotopomer exhibiting a quartet of parallel and perpendicular components. As shown in the spectrum, the weaker $^{71}\text{Ga}^{16}\text{O}$ lines occur at higher magnetic fields for the high field $M_I=-3/2$ transitions and at lower fields for the $M_I=+3/2$ transitions relative to $^{69}\text{Ga}^{16}\text{O}$. All of these transitions exhibited the same, well resolved $^{17}\text{O}(I=5/2)$ sextet hyperfine structure as shown in the highly expanded spectra of Fig. 3 for the highest field Ga transitions ($M_I=-3/2$). The lower spectrum in Fig. 3 shows the perpendicular and much weaker parallel lines for $^{69}\text{Ga}^{16}\text{O}$ and $^{71}\text{Ga}^{16}\text{O}$. Centered about each of these components are the ^{17}O sextets shown in the top spectrum of this figure for $^{69}\text{Ga}^{17}\text{O}$ and $^{71}\text{Ga}^{17}\text{O}$. Since the ^{17}O enrichment is approximately 50%, the central Ga¹⁶O lines also appear in this top spectrum of Fig. 3. Note the amplification factor (X10) increases for the highest field, weakest features, namely, the parallel lines of $^{71}\text{Ga}^{17}\text{O}$. The weak parallel lines of $^{69}\text{Ga}^{17}\text{O}$ were detected but several of these were partially obscured by the more intense $^{71}\text{Ga}^{17}\text{O}$ perpendicular components.

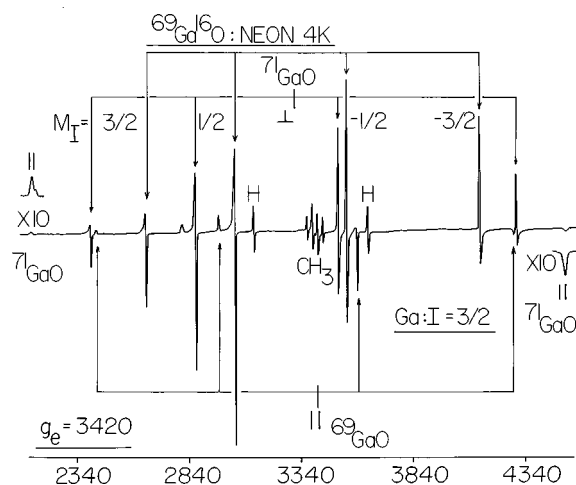


FIG. 2. The overall ESR spectrum of $^{69}\text{Ga}^{16}\text{O}$ and $^{71}\text{Ga}^{16}\text{O}$ isolated in a neon matrix at 4 K is shown. A quartet of parallel ($\theta=0^\circ$) and perpendicular ($\theta=90^\circ$) hyperfine lines is observed for each isotopomer since each gallium isotope has $I=3/2$. Background radical absorptions of H and CH_3 are marked accordingly. This GaO sample was produced by the pulsed laser vaporization of elemental gallium in the presence of O_2 .

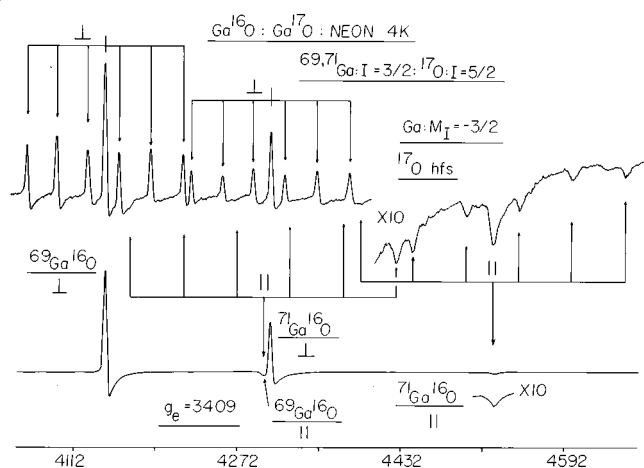


FIG. 3. The lower neon matrix ESR spectrum shows the intense perpendicular ($\theta=90^\circ$) and weaker parallel ($\theta=0^\circ$) lines for the highest field transitions ($M_I=-3/2$) of $^{69}\text{Ga}^{16}\text{O}$ and $^{71}\text{Ga}^{16}\text{O}$. (See overall $^{69,71}\text{Ga}^{16}\text{O}$ spectrum in Fig. 2.) The top spectrum covers this same magnetic field region but for an experiment involving ^{17}O enriched oxygen. The ^{17}O ($I=5/2$) sextet hyperfine structure is clearly observed on the perpendicular lines and is detectable on the weaker parallel features when the signal amplification is increased tenfold as indicated for the highest field region.

Gallium monoxide ESR spectra of this clarity required numerous depositions (approximately 45 separate experiments) in order to optimize the various experimental deposition conditions such as laser power, matrix flow and oxygen concentrations, etc. The spectra unambiguously reveal the presence of one gallium and one oxygen atom in the radical species, hence the assignment to GaO in its $X^2\Sigma$ state seems unequivocal. The observed GaO line positions are listed in Table II and the magnetic parameters in Table III.

C. $^{115}\text{In}^{16}\text{O}$ and $^{115}\text{In}^{17}\text{O}$

The overall simulated ESR spectrum of $^{115}\text{In}^{16}\text{O}$ and its associated H_{RES} vs θ plots for each of the ten hyperfine

TABLE II. ^aObserved ESR line positions (Gauss) for $^{69}\text{Ga}^{16}\text{O}$ and $^{71}\text{Ga}^{16}\text{O}$ in neon matrix at 4 K.

$^{69}\text{Ga}^{16}\text{O}$	Perpendicular ($\theta=90^\circ$)	Parallel ($\theta=0^\circ$)
$I=3/2$		
$M_I=3/2$:	2654	2428
1/2:	3054	2978
-1/2:	3549	3602
-3/2:	4143	4298
$^{71}\text{Ga}^{16}\text{O}$		
$I=3/2$		
$M_I=3/2$:	2406	2137
1/2:	2878	2814
-1/2:	3511	3609
-3/2:	4305	4524

^aMicrowave frequency is 9551.8(4) MHz. Calculated line positions, from an exact diagonalization analysis, agree with these observed lines within the experimental uncertainty of ± 1 Gauss. The magnetic parameters for GaO, extracted from the line positions, are listed in Table III. For Ga^{17}O , sextet hfs for ^{17}O ($I=5/2$) was resolved for both the parallel and perpendicular transitions. See Fig. 3.

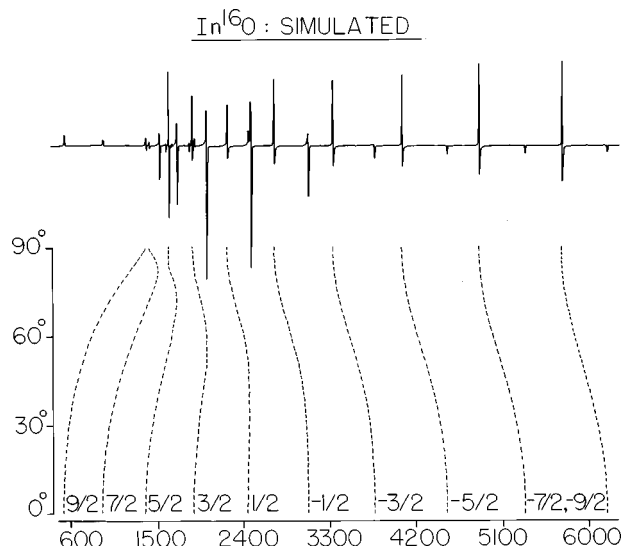


FIG. 4. The overall simulated ESR spectrum of $^{115}\text{In}^{16}\text{O}$ is shown. This complex spectrum can be interpreted by reference to its associated H_{RES} vs θ plots presented directly beneath the spectrum, where θ is the angle between the molecular axis and the externally applied magnetic field. In addition to the expected ten parallel ($\theta=0^\circ$) and ten perpendicular ($\theta=90^\circ$) ^{115}In ($I=9/2$) hyperfine lines, several extra absorption features are seen to occur at off-angle positions. Only H_{RES} vs θ features having significant transition probabilities are shown. Note that the $^{115}\text{In}^{16}\text{O}$ absorptions extend over the extremely large range of approximately 500–6200 Gauss.

transitions of ^{115}In ($I=9/2$) are presented in Fig. 4. This InO ESR spectrum is a most interesting diatomic radical example which could not be thoroughly analyzed without the assistance of simulated comparisons. The spectrum is especially

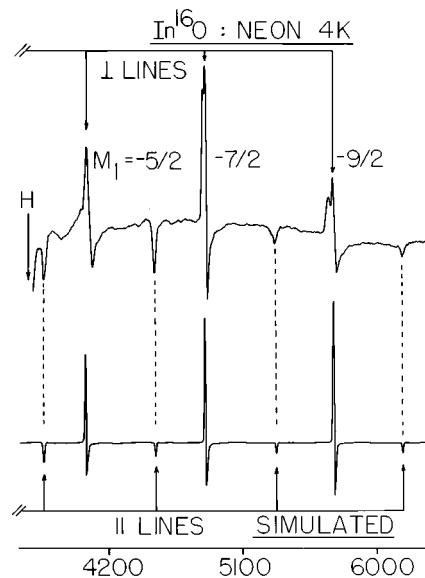


FIG. 5. The three highest field ^{115}In ($I=9/2$) hyperfine transitions observed in a neon matrix ESR spectrum of $^{115}\text{In}^{16}\text{O}$ are shown for both the parallel (||) and perpendicular (\perp) components. The simulated ESR spectrum is shown below the observed. See Fig. 4 for the overall ESR spectrum of $^{115}\text{In}^{16}\text{O}$. The applied magnetic field is given in Gauss. The absorption feature labeled “H” is the high field transition of the hydrogen atom doublet hyperfine pattern.

TABLE III. ^aObserved magnetic parameters for Al^{17}O , $^{69,71}\text{Ga}^{17}\text{O}$, and $^{115}\text{In}^{17}\text{O}$ in their $X^2\Sigma$ ground states in neon matrices at 4 K.

	g_{\parallel}	g_{\perp}	$^bA_{\parallel}$	$^bA_{\perp}$	$^cA_{\text{dip}}$	$^cA_{\text{iso}}$
Al^{16}O :	2.0020	2.0011	871	714	52 (61)	766 (540)
^{17}O :			-98	52	-50 (-65)	2 (9)
$^{69}\text{Ga}^{16}\text{O}$:	1.9990	1.9680	1736	1356	127 (123)	1483 (648)
$^{71}\text{Ga}^{16}\text{O}$:	1.9990	1.9680	2207	1722	162 (156)	1884 (823)
^{17}O :			-145	85	-77 (-89)	8 (2)
$^{115}\text{In}^{16}\text{O}$:	1.975 (3)	1.810 (2)	1728 (3)	1188 (2)	180 (173)	1368 (523)
^{17}O :			-228	166	-131 (-90)	35 (-4)

^aAll A values are in MHz. Experimental uncertainties are approximately ± 0.0002 in the g values and ± 1 MHz in the A values unless otherwise noted. A_{iso} and A_{dip} are defined in the text.

^bThe signs of the metal A values are clearly positive based upon their large magnitudes. The indicated signs for the ^{17}O A values were selected to yield the closest agreement with the theoretical calculations for A_{iso} and A_{dip} .

^cThe A_{dip} and A_{iso} values shown in parenthesis were calculated using UB3LYP, a density functional approach. See Table IV. The negative sign of the nuclear magnetic moment for ^{17}O is reflected in the ^{17}O A values listed in this table.

complex at low magnetic fields since the inherent g and A tensor anisotropies, coupled with the large $I=9/2$ value, produce “extra” or off-angle absorptions on the $M_I=7/2, 5/2, 3/2,$ and $1/2$ hyperfine transitions (see Table V). Also the two lowest field perpendicular lines are extremely weak and occur very close together. These spectral properties are consistent with the nature of the H_{RES} vs Θ plots shown in Fig. 4.

The high field region of the $^{115}\text{In}^{16}\text{O}$ spectrum is straight forward to interpret and is shown in Fig. 5 where the experimental spectrum is compared directly with a simulated spectrum. The magnetic parameters employed to produce this close fit between simulated and observed spectra are listed in Table III. The intensity variations of the individual hyperfine lines are strongly influenced by varying degrees of overlap of ^{115}InO lines in different matrix trapping sites which have slightly different A and g values. As usual, these matrix site effects varied greatly among the different depositions and were partially removed by annealing the neon matrix (warming briefly to 9 K and recooling to 4 K).

Extremely clear and well-resolved $^{17}\text{O}(I=5/2)$ sextet hyperfine structure was observed for $^{115}\text{In}^{17}\text{O}$ as shown in Fig. 6 for the parallel and perpendicular ^{115}In : $M_I=-7/2$ high field transition. The same ^{17}O perpendicular and parallel splittings were observed on the other intense features of

$^{115}\text{In}^{17}\text{O}$. The magnetic parameter for $^{115}\text{In}^{17}\text{O}$ are listed in Table III.

As discussed below, only a tentative assignment for $^{115}\text{In}^{16}\text{O}$ in argon matrices was possible given the difficulties of obtaining sufficiently intense ESR signals in this host. A tentative assignment of the $^{115}\text{In}^{16}\text{O}$ argon magnetic parameters are: $g_{\parallel}=1.982(4)$; $g_{\perp}=1.811(3)$; $A_{\parallel}=1765(10)$; and $A_{\perp}=1205(7)$ MHz. These show close agreement with the neon results, and like AlO , exhibit larger A values in argon relative to neon.

IV. DISCUSSION

The neon magnetic parameters for $^{27}\text{Al}^{16}\text{O}$, produced in these experiments by reactive pulsed-laser vaporization, agree within experimental uncertainty with the earlier results where the AlO radical was generated by conventional high temperature vaporization of $\text{Al}_2\text{O}_3(\text{s})$ at 2500 K from a standard effusion oven.¹ One other example where a detailed comparison between these two quite different generation methods for the study of high temperature species has been made is the $\text{BF}^+(X^2\Sigma)$ radical.⁴² Since the initial matrix ESR measurements of the aluminum hyperfine interactions were reported, gas phase results have become available.² As

TABLE IV. ^aCalculated nuclear hyperfine properties for AlO , GaO , and InO in their $X^2\Sigma$ states.

Radical	Method	E	$A_{\text{iso}}(M)$	$A_{\text{dip}}(M)$	$A_{\text{iso}}(^{17}\text{O})$	$A_{\text{dip}}(^{17}\text{O})$	^b Basis	g_N	R	^c $q(M)$	^c $q_s(M)$	^c $\langle S^2 \rangle$
$^{27}\text{Al}^{17}\text{O}$	UHF	-316.7785	-466	61	-41	-106	$22s, 16p, 4d$	1.4565	1.6179	0.612	0.014	0.812
	UB3LYP	-317.6817	540	61	9	-65				0.732	0.489	0.758
$^{69}\text{Ga}^{17}\text{O}$	UHF	-1998.1415	-1048	118	-33	-106	$22s, 17p, 12d$	1.3430	1.7436	0.589	0.059	0.805
	UB3LYP	-2000.1706	648	123	2	-89				0.598	0.313	0.761
$^{115}\text{In}^{17}\text{O}$	UHF	-5814.9759	-1440	163	-55	-112	$23s, 18p, 13d$	1.2300	1.8768	0.878	0.079	0.804
	UB3LYP	-5817.8483	523	173	-4	-90				0.878	0.306	0.763

^a A values reported in MHz, R in Å, and energy (E) in hartrees. The nuclear g factor is denoted by g_N and has a value of -0.7575 for ^{17}O . The A_{iso} and A_{dip} parameters are defined in the text. The density functional theory method is designated UB3LYP.

^bThe oxygen basis set was $21s, 15p, 4d$. All basis functions were uncontracted, spherical harmonic Gaussians.

^c $q(M)$ is total charge on metal; $q_s(M)$ in total spin density on metal; $\langle S^2 \rangle$ reflects the degree of spin contamination of the wave function. For pure doublet states, the expected value is 0.75.

TABLE V. ^aObserved ESR line positions (Gaussian) for $^{115}\text{In}^{16}\text{O}$ in neon matrix at 4 K.

	Parallel ($\theta=0^\circ$)	Off angle	Perpendicular ($\theta=90^\circ$)
$^{115}\text{In}: I=9/2$			
$M_I=9/2$	523	...	1358
7/2	920	1482 (81°)	1390
5/2	1362	1667 (72°)	1589
3/2	1859	1980 (57°)	1834
1/2	2419	2440 (36°)	2199
-1/2	^b 3046	...	2692
-3/2	3741	...	^b 3309
-5/2	4499	...	4033
-7/2	5312	...	4840
-9/2	6171	...	5708

^aThe microwave frequency is 9587.0(4) MHz. Given the larger linewidths of these ^{115}InO absorptions, the experimental uncertainty is approximately ± 3 Gauss. All lines, including the “extra” or off-angle features were fitted with our exact diagonalization program using the magnetic parameters listed in Table III.

^bThese lines were obscured by intense background absorptions.

is usually the case, the neon results show the closest agreement with the gas phase values. The gas phase, neon, argon, and krypton A_{iso} values for ^{27}Al in $^{27}\text{Al}^{16}\text{O}$ are 738.0(14), 766(2), 899(3), and 920(3) MHz, respectively. The ^{27}Al dipolar parameters (A_{dip}), listed in the same order are, 56.392(82), 53.0(7), 54(1), and 51(1) MHz.

For A_{iso} , these comparisons show a neon-gas shift of 3.8% and an argon shift of 22%. The A_{dip} parameter is some-

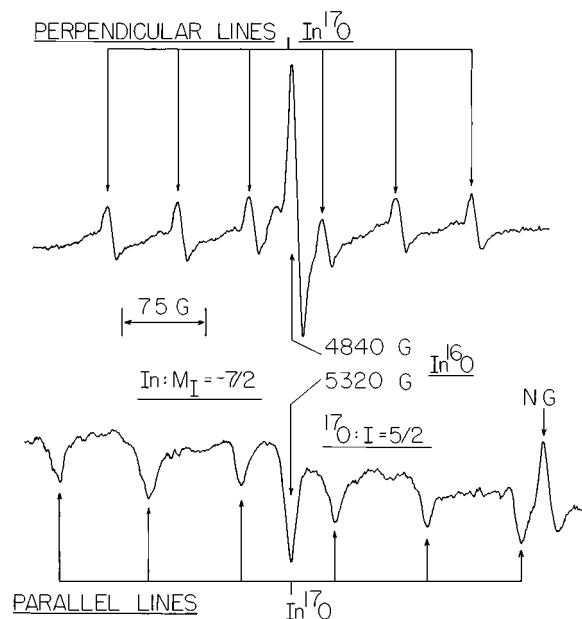


FIG. 6. The $^{17}\text{O}(I=5/2)$ hyperfine structure associated with the parallel and perpendicular components of the $^{115}\text{In}: M_I = -7/2$ transition is shown for the $^{115}\text{In}^{17}\text{O}$ radical. The unsplit central features result from $^{115}\text{In}^{16}\text{O}$ radicals which are also present in this neon matrix sample. The up-phase absorption feature labelled “NG” (lower right) results from the beginning of the “next group” of perpendicular lines associated with the $^{115}\text{In}: M_I = -9/2$ transition for the $^{115}\text{In}^{17}\text{O}$ radical. The signal amplification factor for the weaker parallel spectrum (lower trace) was four times that employed for the more intense perpendicular components (upper trace).

what less dependent on the particular matrix host. Since the nuclear hyperfine interaction for only a very small number of high temperature radicals has been resolved in the gas phase, this AIO comparison is especially valuable. It also implies that these new neon results for GaO and InO should be close, within a few percent, of the gas phase values. This assumption will be an important consideration when detailed experimental-theoretical comparisons are made in the following section of this article.

The matrix isolation Fourier transform infrared (FTIR) vibrational studies using the reactive laser vaporization method have detected BO and AIO in argon but not GaO and InO.^{19,20} However, reaction products presumably resulting from the heavier MO molecules under these conditions were detected, for example M_2O_2 . Neon matrix vibrational experiments were apparently not conducted. Consistent with the argon vibrational results, we were able to obtain only weak InO and no GaO argon matrix ESR spectra despite numerous experimental attempts under a variety of experimental conditions. Both direct and indirect encounters between $\text{O}_2(g)$ and laser-ablated metal were tried over wide concentration ranges. In the direct scheme, pure $\text{O}_2(g)$ is passed directly over the metal undergoing laser vaporization. The indirect method involves the introduction of $\text{O}_2(g)$ as a dopant in the rare gas flow, hence encounters between metal atoms and $\text{O}_2(g)$ occur predominantly during the matrix condensation process. The difficulties of detecting GaO and InO in argon matrices by both ESR and IR spectroscopy is puzzling. Reaction between O_2 and these heavier metals might depend upon excited state encounters. Hence, more efficient excited state quenching by the heavier rare gases might account for these observations. The smaller atomic and molecular diffusion rates in argon relative to neon might also be an important difference.

The conversions from the observed ESR hyperfine parameters (A_{\parallel} and A_{\perp}) to the properties (A_{iso} and A_{dip}) that are required to establish electronic structure trends among these diatomic oxide radicals are conducted with the following relationships:

$$A_{\text{iso}} = 8/3 \pi g_e g_n \beta_e \beta_n \langle \delta(r) \rangle = (2A_{\perp} + A_{\parallel})/3$$

$$A_{\text{dip}} = 1/2 g_e g_n \beta_e \beta_n \langle (3 \cos^2 \theta - 1)/r^3 \rangle = (A_{\parallel} - A_{\perp})/3,$$

where all symbols have their standard definitions and the averages are taken over the spin densities.²⁵ The small $\vec{L} \cdot \vec{I}$ terms are neglected since the g values do not differ substantially from g_e .

V. ELECTRONIC STRUCTURE TRENDS

These experimental A_{iso} and A_{dip} values for a specific nucleus in a molecular radical can be compared to a set of calculated free atom parameters to yield estimates of valence “ s ” and “ p_z ” orbital characters, respectively. The free atom comparison method (FACM) results using a commonly applied set of atomic values⁴³ for BO, AIO, GaO, and InO are listed in Table VI where both metal and oxygen valence

TABLE VI. ^aFree atom comparison method (FACM) results for the MO diatomic radicals: valence electronic structure trends.

	Metal				Oxygen (^{17}O)				$^f\Sigma$ TOTAL
	A_{iso}	A_{dip}	$X(ns)$	$X(np_z)$	A_{iso}	A_{dip}	$X(2s)$	$X(2p_z)$	
$^{b11}\text{B}^{17}\text{O}$	1033	25	0.41	0.39	-19 (3)	-12 (3)	0.004	0.07	0.87
$^c\text{Gas phase}$	1027.4	27.1							
$^{d27}\text{Al}^{17}\text{O}$	766	52	0.20	0.63	2	-50	-0.0004	0.30	1.13
$^c\text{Gas phase}$	738.0	56.4							
$^{d69}\text{Ga}^{17}\text{O}$	1483	127	0.12	0.62	8	-77	-0.002	0.46	1.20
$^{d115}\text{In}^{17}\text{O}$	1368 (3)	180 (3)	0.07	0.63	35	-131	-0.007	0.78	1.48

^a A values reported in MHz. See text for A_{iso} and A_{dip} definitions and the sign choices for the A values. The valence orbital characters (X) are obtained by a simple comparison with a standard set of free atom A_{iso} and A_{dip} values. (Ref. 43) Unless otherwise indicated all A values are from neon matrix ESR measurements and have an experimental uncertainty of ± 1 MHz.

^bRef. 3.

^cRef. 4.

^dThis work.

^eRef. 2.

^fA discussion as to why some of these totals exceed unity is given in the text.

orbital characters are shown. A detailed analysis of inaccuracies that can arise with this simple FACM treatment have been thoroughly discussed in an earlier study of several diatomic radicals, including AlO and its isoelectronic cation, SiO^+ .⁴⁴ A major source of error is introduced into FACM when “core-other valence overlap” is significant. This effect, which is not spin polarization, was shown to be large for oxygen $2p_z$ overlap with the inner shells of aluminum. The FACM values for Al in AlO, $3s=0.20$ and $3p_z=0.63$, needed to be adjusted to 0.41 and 0.26, respectively.⁴⁴ Hence, the FACM s/p_z ratio changed from 0.32 to 1.58 after this effect and others were included in the theoretical analysis.

The origin of the core-other valence overlap effect is briefly described for the $A-B$ diatomic radical. Orthogonalizing the valence orbitals of A to the core of B introduces nonzero coefficients multiplying the core orbitals of B into the valence MOs. Because of the definition of the Mulliken population, these core orbitals make no contribution to the Mulliken population. When the valence MO is evaluated at the B nucleus, however, the core orbital part of the valence MO makes a large contribution. This makes the FACM result of dividing the spin density by the valence spin density of the atom an unreliable method for determining spin populations.

It is highly significant that the oxygen A values, which were not available at the time of the earlier $\text{Al}^{16}\text{O}/\text{Si}^{16}\text{O}^+$ study, yield FACM $2s$ and $2p_z$ characters that show nearly exact agreement with the earlier calculated (CI) results of $2s \approx 0$ and $2p_z = 0.30$. Since the oxygen $2p_z$ character is not affected by core-other valence overlap effects, the FACM values for this parameter should provide a more accurate description of the bonding trend for this series of metal oxide radicals. Going from B^{17}O to In^{17}O , the oxygen $2p_z$ character increases in the order 0.07, 0.30, 0.46, and 0.78. As expected, the oxygen $2s$ character is nearly zero for all four MO radicals.

The large increases in the oxygen $2p_z$ character going

down the group would seem to reflect an overall electronic shift from $\text{M}^{++}\text{O}^{--}$ to M^+O^- . Certainly, the experimental trend in the ^{17}O A_{dip} parameters does indicate that considerably more spin density does reside on oxygen going down the group but this alone does not necessarily require large shifts in the overall charge—a topic that is discussed more fully in the theoretical section.

Although we have not conducted as high a level of orbital population analysis and calculation for GaO and InO as was done earlier for AlO, it would not be surprising to also find a large core-other valence overlap effect operative in the heavier oxides. Inclusion of the effect would most probably reduce the large np_z metal characters predicted by FACM by a significant amount. This seems reasonable since the sum of the valence characters for GaO (1.20) and InO (1.48) are considerably greater than unity and large corrections to the oxygen $2p_z$ characters are not warranted, given the absence of an inner “ p ” shell. A Mulliken population analysis of the DFT Slater determinant with the extended basis set is subject to many criticisms. For what it is worth, it shows that the spin density for GaO has $0.1s$, $0.24p$ on Ga and $0.1s$ and $0.55p$ on O. This agrees with the idea that the neutral p character on the metal is overestimated by FACM, but the oxygen is reasonable. Based upon FACM predictions alone, the metal ns valence character decreases in the order 0.41, 0.20, 0.12, and 0.07 going down the group, BO to InO. Without extensive calculations on these heavier oxides with extremely complicated inner-shell effects, it is difficult to judge how these FACM estimates of the ns character should be adjusted.

The theoretical calculations of A_{iso} and A_{dip} for the metal atoms and oxygen are given in Table III in parenthesis alongside the experimental results. A detailed description of these calculations is provided in the next section. Agreement between theory (UB3LYP) and experiment is quite good for the A_{dip} values in all cases except for oxygen in the AlO and InO cases, and even there, the agreement is within 33%. Deviation between observed and calculated metal A_{iso} values

increases from -30% in AlO to -62% in InO.

The increasing negative deviation of the g_{\parallel} and g_{\perp} values from g_e going down this MO radical series (see Table III) reflects the large increases in the spin-orbit coupling parameters of the metal atoms and possible changes in the nature of the excited $^2\Pi$ states. Spin-orbit coupling between the ground $X^2\Sigma$ electronic states and excited $^2\Pi$ states can become quite complicated since both $^2\Pi_i$ and $^2\Pi_r$ types are involved, and these two types shift the g values in opposite directions.⁷ Whether the excited $^2\Pi$ states are similar in GaO and InO, for example, can be estimated by determining if $\Delta g_{\perp}(g_{\perp} - g_e)$ is merely reflecting changes in the metal atom spin-orbit parameters (λ). As shown by the g tensor data in Table III, the Δg_{\perp} ratio for InO/GaO is 5.6 compared to a spin-orbit ratio of 2.7 for these two metals. Hence, the greater than expected g_{\perp} shift for InO, based on λ alone, implies that the $^2\Pi_r$ state is more strongly coupled to the ground $^2\Sigma$ state relative to GaO.

VI. THEORETICAL RESULTS

Calculations for AlO, GaO, and InO were performed with an extended basis set⁴⁵ using the MELD⁴⁶ and GAUSSIAN94⁴⁷ programs in order to compare theoretical estimates of the nuclear hyperfine properties with these neon matrix experimental results (see Table IV). For AlO, the results were generally unstable with respect to the quality of the CI calculation. The spin density at the metal nucleus, especially, varied greatly with method.

For AlO, Yoshimine *et al.*⁴⁸ have pointed out that there are two solutions to the (ROHF) equations with nearly equal energy, and that the one obtained depends on the initial guess. The spin density for AlO has also been calculated in two of our previous articles^{44,49} using CI methods and iterative natural orbitals, but with smaller basis sets. These previous calculations gave reasonable ($\pm 50\%$) agreement with the aluminum A_{iso} value. With the present large uncontracted basis, the value of A_{iso} at Al was $+3$ MHz but with a contraction of the tightest s and p functions, the value jumped to $+1110$ MHz. The UHF value with the uncontracted basis is -416 MHz and single double configuration interaction (SDCI), which includes most of the spin polarization effects, likewise gave a negative value with both basis sets. Very large multireference single double configuration interaction (MRSDCI) with either basis gave positive values for A_{iso} in the 100–300 MHz range with the uncontracted basis and the 700–900 MHz range with the contracted basis.

Density functional theory with spin-dependent generalized gradient functionals has been found empirically⁵⁰ to give reasonable spin densities for many systems including those with heavy metals. The uncontracted basis and the B3LYP^{51,52} method applied to AlO gave 540 MHz for A_{iso} which shows better agreement with experiment than any of the CI calculations with the same basis. For GaO, the results were similar. The ROHF $A_{\text{iso}}(^{69}\text{Ga})$ was $+35$ MHz, while the largest MRSDCI yielded -47 MHz. By contrast, the UHF result was -1048 MHz and B3LYP gave $+648$ MHz.

The calculated A_{dip} values for the metal and oxygen us-

ing the DFT (UB3LYP) method show reasonable agreement with experiment as shown by the comparison data of Table III. For example, A_{dip} for Al in AlO is calculated to be 61 MHz compared to the observed value in neon of 52 MHz. Even for InO, the metal's observed A_{dip} value of 180 MHz shows good agreement with the calculated value of 173 MHz.

Past results for AlO and SiO^+ have already demonstrated^{44,49} that these were very difficult molecules for spin density calculations. The MO molecule is actually best described as somewhere between $\text{M}^{++}\text{O}^{--}$ with the unpaired electron in the metal s orbital and M^+O^- with the unpaired electron in the oxygen sp hybrid orbital polarized away from the metal. Without a proper description of electron correlation, the $\text{M}^{++}\text{O}^{--}$ configuration lies too high in energy relative to M^+O^- so the wave function is biased towards M^+O^- . Obviously the A values measured in the ESR experiment are extremely sensitive to this balance. Since these two configurations differ nominally by a single excitation, $\sigma(\text{M})^2\alpha(\text{O})^1 \rightarrow \sigma(\text{M})^1\sigma(\text{O})^2$, they have no connecting matrix element in the CI. Mixing between them, in the CI, is described by coupling through a large number of double excitations. Consequently, MRSDCI is not very effective since no small reference space brings in the single excitation to the correct extent. MRSDCI works best when all of the coefficients in the reference space are well represented by first order perturbation theory.

Because these two configurations can always be rewritten as a single Slater determinant, methods like DFT that build the effect of electron correlation into an effective potential can obtain an improved spin density from a single determinant model. Certainly in this case, the spin density is greatly improved. On the other hand, agreement with experiment is still far from perfect. Examination of the Mulliken charges shows, however, that the charge on the metal is not greatly affected by going from UHF to UB3LYP. Rather, the spin density change is associated with a redistribution of the singly occupied orbital compensated by a shift in the other direction of the doubly occupied orbitals so that the charge distribution remains nearly unchanged. For example, the initial p electron on the free metal atom in its 2P ground state goes into forming a π bond with the oxygen. The polarity of this π bond is not directly measured by ESR, but is indirectly connected to the distribution of σ electrons.

It is dangerous to compare Mulliken charge between different molecules because (a) the extended basis sets with diffuse functions are only nominally associated with each atom and (b) density functional theory yields a density but does not give a density matrix. Like $\langle S^2 \rangle$, the Mulliken population relies on treating the Slater determinant formed from DFT orbitals as if it were an actual wave function.

ACKNOWLEDGMENTS

Support of the National Science Foundation (LBK: CHE-9319291) and (ERD: CHE-9526161) is gratefully acknowledged. A Duke Endowment grant to Furman University and a Research Corporation Cottrell College Science

Award (L.B.K.) also provided valuable support for this project. The authors would like to express their appreciation to Robert Babb and Edward Earl for providing important computer assistance in various stages of this work.

- ¹L. B. Knight, Jr. and W. Weltner, Jr., *J. Chem. Phys.* **55**, 5066 (1971).
- ²C. Yamada, E. A. Cohen, M. Fujitake, and E. Hirota, *J. Chem. Phys.* **92**, 2146 (1990).
- ³L. B. Knight, Jr., J. O. Herlong, T. J. Kirk, and C. A. Arrington, *J. Chem. Phys.* **96**, 5604 (1992).
- ⁴M. Tanimoto, S. Saita, and E. Hirota, *J. Chem. Phys.* **84**, 1210 (1986).
- ⁵B. H. Lengsfeld III and B. Liu, *J. Chem. Phys.* **77**, 6083 (1982).
- ⁶W. Weltner, Jr., D. McLeod, and P. H. Kasai, *J. Chem. Phys.* **46**, 3172 (1967).
- ⁷K. P. Huber and G. Herzberg, *Constants of Diatomic Molecules (IV)* (Van Nostrand Reinhold, New York, 1979); P. J. Dagdigian, H. W. Cruse, and R. N. Zare, *J. Chem. Phys.* **62**, 1824 (1975).
- ⁸M. Cai, C. C. Carter, T. A. Miller, and V. E. Bondybey, *J. Chem. Phys.* **95**, 73 (1991).
- ⁹D. E. Clemmer, M. E. Weber, and P. B. Armentrout, *J. Chem. Phys.* **96**, 10 888 (1992).
- ¹⁰D. P. Belyung, A. Fontijn, and P. Marshall, *J. Phys. Chem.* **97**, 3456 (1993).
- ¹¹G. A. Slavejkov, C. T. Clyde, and A. Fontijn, *J. Phys. Chem.* **94**, 3347 (1990).
- ¹²A. P. Salzberg, D. I. Santiago, F. Asmar, D. N. Sandoval, and B. R. Weiner, *Chem. Phys. Lett.* **180**, 161 (1991).
- ¹³M. L. Campbell, R. E. McClean, N. L. Garland, and H. H. Nelson, *Chem. Phys. Lett.* **194**, 187 (1992).
- ¹⁴M. Singh, *Astrophys. Space Sci.* **140**, 421 (1988).
- ¹⁵H. Partridge, S. R. Langhoff, B. H. Lengsfeld III, and B. Liu, *J. Quant. Spectrosc. Radiat. Transf.* **30**, 449 (1983).
- ¹⁶H. R. Johnson and A. J. Sauval, *Astron. Astrophys. Suppl. Ser.* **49**, 77 (1982).
- ¹⁷J. A. Coxon and S. Naxakis, *J. Mol. Spectrosc.* **111**, 102 (1985).
- ¹⁸R. W. Dreyfus, R. Kelly, and R. E. Walkup, *Appl. Phys. Lett.* **49**, 1478 (1986).
- ¹⁹L. Andrews, T. R. Burkholder, and J. T. Yustein, *J. Phys. Chem.* **96**, 10 182 (1992).
- ²⁰T. R. Burkholder, J. T. Yustein, and L. Andrews, *J. Phys. Chem.* **96**, 10 189 (1992).
- ²¹S. J. Bares, M. Haak, and J. W. Nibler, *J. Chem. Phys.* **82**, 670 (1985).
- ²²S. J. Bares and J. W. Nibler, *J. Mol. Struct.*, **157**, 215 (1987).
- ²³A. J. Hinchcliffe and J. S. Ogden, *J. Phys. Chem.* **77**, 2537 (1973).
- ²⁴M. A. Douglas, R. H. Hauge, and J. L. Margrave, *High Temp. Sci.* **16**, 35 (1983); M. A. Douglas, R. H. Hauge, and J. L. Margrave, *J. Am. Chem. Soc.* **102**, 6005 (1980).
- ²⁵W. Weltner, Jr., *Magnetic Atoms and Molecules* (Dover, Mineola, New York, 1989).
- ²⁶L. B. Knight, Jr., G. C. Jones, G. M. King, R. M. Babb, and A. J. McKinley, *J. Chem. Phys.* **103**, 497 (1995).
- ²⁷L. B. Knight, Jr., R. Babb, M. Ray, T. J. Banisaukas III, L. Russon, R. S. Dailey, and E. R. Davidson, *J. Chem. Phys.* **105**, 10 237 (1996).
- ²⁸L. B. Knight, Jr., S. T. Cobranchi, B. W. Gregory, and E. Earl, *J. Chem. Phys.* **86**, 3143 (1987).
- ²⁹L. B. Knight, Jr., E. Earl, A. R. Ligon, D. P. Cobranchi, J. R. Woodward, J. M. Bostick, D. R. Davidson, and D. Feller, *J. Am. Chem. Soc.* **108**, 5065 (1986).
- ³⁰L. B. Knight, Jr., S. T. Cobranchi, J. O. Herlong, and C. A. Arrington, *J. Chem. Phys.* **92**, 5865 (1990).
- ³¹L. B. Knight, Jr., J. R. Woodward, T. J. Kirk, and C. A. Arrington, *J. Phys. Chem.* **97**, 1304 (1993).
- ³²Y. M. Hamrick, R. J. Van Zee, and W. Weltner, Jr., *J. Chem. Phys.* **96**, 1767 (1992).
- ³³J. M. Parnis and G. A. Ozin, *J. Phys. Chem.* **93**, 1215 (1989); **93**, 1204 (1989); G. Jeong and K. J. Klabunde, *J. Am. Chem. Soc.* **108**, 7103 (1986).
- ³⁴P. H. Kasai and P. M. Jones, *J. Am. Chem. Soc.* **106**, 8018 (1984).
- ³⁵L. B. Knight, Jr. and J. T. Petty, *J. Chem. Phys.* **88**, 481 (1988).
- ³⁶J. A. Howard and B. Mile, *Acc. Chem. Res.* **20**, 173 (1987).
- ³⁷L. B. Knight, Jr., J. J. Banisaukas III, R. Babb, and E. R. Davidson, *J. Chem. Phys.* **105**, 6607 (1996).
- ³⁸R. J. Van Zee, S. Li, and W. Weltner, Jr., *J. Chem. Phys.* **98**, 4335 (1993).
- ³⁹P. M. Jones and P. J. Kasai, *J. Phys. Chem.* **92**, 1060 (1988).
- ⁴⁰P. Pullumbi, C. Mijoule, L. Manceron, and Y. Bouteiller, *Chem. Phys.* **185**, 13 (1994).
- ⁴¹L. B. Knight, Jr., *Radical Ionic Systems*, edited by A. Lund and M. Shiotani (Kluwer Academic, New York, 1991), pp. 73–97.
- ⁴²L. B. Knight, Jr., A. Ligon, S. T. Cobranchi, D. P. Cobranchi, E. Earl, D. Feller, and E. R. Davidson, *J. Chem. Phys.* **85**, 5437 (1986).
- ⁴³J. R. Morton and K. R. Preston, *J. Magn. Reson.* **30**, 577 (1978).
- ⁴⁴L. B. Knight, Jr., A. Ligon, R. W. Woodward, D. Feller, and E. R. Davidson, *J. Am. Chem. Soc.* **107**, 2857 (1985).
- ⁴⁵H. Partridge, NASA Technical Memorandum 101 044, 1989. The largest basis sets from this source were used for gallium ($21s16p10d$), supplemented by one additional diffuse s , p , and two additional diffuse d functions. For aluminum, the Partridge $20s15p$ basis was supplemented by two additional diffuse s , one additional p , and four d polarization functions. For oxygen, three additional s , two additional p , and four d polarization functions were added to his $18s13p$ set. For indium, no optimized basis was available, so the s , p basis of gallium was scaled by 1.6 (the ratio of nuclear charges) and the d basis was scaled by 2.0. Three additional s , 2 additional p , and one additional d function were added to cover the additional valence shell.
- ⁴⁶MELD is a set of electronic structure programs written by L. E. McMurchie, S. T. Elbert, S. R. Langhoff, and E. R. Davidson, with extensive modifications by D. Feller and D. C. Rawlings.
- ⁴⁷GAUSSIAN94, M. J. Frisch, G. W. Trucks, H. B. Schlegel, P. M. W. Gill, B. G. Johnson, M. A. Robb, J. R. Cheeseman, T. A. Keith, G. A. Peterson, J. A. Montgomery, K. Raghavachari, M. A. Al-Laham, V. G. Zakrzewski, J. V. Ortiz, J. B. Foresman, J. Cioslowski, B. B. Stefanov, A. Nanayakkara, M. Challacombe, C. Y. Peng, P. Y. Ayala, W. Chen, M. W. Wong, J. L. Andres, E. S. Replogle, R. Gomperts, R. L. Martin, D. J. Fox, J. S. Binkley, D. J. Defrees, J. Baker, J. P. Stewart, M. Head-Gordon, C. Gonzalez, and J. A. Pople (Gaussian, Inc., Pittsburgh, PA, 1995).
- ⁴⁸M. Yoshimine, A. D. McLean, and B. Liu, *J. Chem. Phys.* **58**, 4412 (1973).
- ⁴⁹L. B. Knight, Jr., M. B. Wise, E. R. Davidson, and L. E. McMurchie, *J. Chem. Phys.* **76**, 126 (1982); L. B. Knight, Jr., J. O. Herlong, T. J. Kirk, and C. A. Arrington, *J. Chem. Phys.* **96**, 5604 (1992).
- ⁵⁰E. R. Davidson and R. F. Frey, *J. Chem. Phys.* **106**, 2331 (1997).
- ⁵¹A. D. Becke, *J. Chem. Phys.* **98**, 5648 (1993); A. D. Becke, *Phys. Rev. A* **38**, 3098 (1988).
- ⁵²C. Lee, W. Yang, and R. G. Parr, *Phys. Rev. B* **37**, 785 (1988); B. Miehlich, A. Savin, H. Stoll, and H. Preuss, *Chem. Phys. Lett.* **157**, 200 (1989).